Complex Refractive Index Spectra of CH₃NH₃PbI₃ Perovskite Thin Films Determined by Spectroscopic Ellipsometry and Spectrophotometry

Philipp Löper,*,[†] Michael Stuckelberger,[†] Bjoern Niesen,[†] Jérémie Werner,[†] Miha Filipič,[‡] Soo-Jin Moon,[§] Jun-Ho Yum,[§] Marko Topič,[‡] Stefaan De Wolf,[†] and Christophe Ballif[†,§]
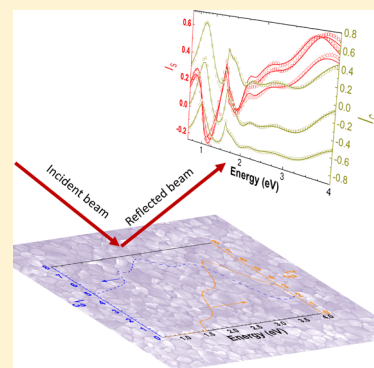
[†]École Polytechnique Fédérale de Lausanne (EPFL), Institute of Microengineering (IMT), Photovoltaics and Thin-Film Electronics Laboratory, Rue de la Maladière 71b, 2002 Neuchâtel, Switzerland
[‡]Faculty of Electrical Engineering, University of Ljubljana, Tržaška 25, 1000 Ljubljana, Slovenia
[§]CSEM SA, PV-center, Jaquet-Droz 1, 2002 Neuchâtel, Switzerland

 Ⓢ *Supporting Information*

ABSTRACT: The complex refractive index (dielectric function) of planar CH₃NH₃PbI₃ thin films at room temperature is investigated by variable angle spectroscopic ellipsometry and spectrophotometry. Knowledge of the complex refractive index is essential for designing photonic devices based on CH₃NH₃PbI₃ thin films such as solar cells, light-emitting diodes, or lasers. Because the directly measured quantities (reflectance, transmittance, and ellipsometric spectra) are inherently affected by multiple reflections, the complex refractive index has to be determined indirectly by fitting a model dielectric function to the experimental spectra. We model the dielectric function according to the Forouhi−Bloomer formulation with oscillators positioned at 1.597, 2.418, and 3.392 eV and achieve excellent agreement with the experimental spectra. Our results agree well with previously reported data of the absorption coefficient and are consistent with Kramers−Kronig transformations. The real part of the refractive index assumes a value of 2.611 at 633 nm, implying that CH₃NH₃PbI₃-based solar cells are ideally suited for the top cell in monolithic silicon-based tandem solar cells.

Organic−inorganic perovskites have recently attracted strong interest as a solar cell absorber material as perovskite-based solar cells have attained within only a few years impressive energy conversion efficiencies with certified values under standard test conditions of up to 20.1%.[1−3] Methylammonium lead triiodide (CH₃NH₃PbI₃), the material used in the most efficient perovskite solar cells, has a bandgap (E_G) of ~1.57 eV,[4,5] a very sharp absorption edge,[6] and an impressively low difference between open-circuit voltage (V_{OC}) and its bandgap potential (E_G/q).[6−8] Organic−inorganic perovskites have also been identified as a promising solid state lighting material[9] and for lasing applications[10−13] and have been employed for thin-film electronic devices as well.[14−16] The bandgap and high photovoltaic efficiencies also render organic−inorganic perovskites a suitable material for tandem solar cells, which represent the most straightforward way to overcoming the efficiency limits of established bottom cell technologies, such as crystalline silicon (c-Si) or copper indium gallium diselenide (CIGS), or emerging technologies such as kesterites.[3,7,17,18] While the potential of CH₃NH₃PbI₃/c-Si tandems has already been pointed out, all investigations have so far relied on postulated and spectrally constant refractive index data for CH₃NH₃PbI₃, as refractive index spectra were not yet available.[19−21]

Perovskite-based photonic devices such as light-emitting diodes, lasers, and single-junction or tandem solar cells consist of thin-film layer stacks that manage light in- and out-coupling as well as charge carrier injection or extraction. For a thorough optical design of multilayer photonic devices, detailed knowledge of the complex refractive index (dielectric function) over the full relevant spectral range is essential.

So far, only very limited information on the optical and dielectric properties of CH₃NH₃PbI₃ is available. Most investigations focused on the low-frequency range, that is, frequency <1 MHz[22−24] and from 50 to 150 GHz.[25] For the visible spectral range, a dielectric constant of 6.5 at a temperature of 4.2 K was reported.[26] Moreover, the absorption coefficient of CH₃NH₃PbI₃, measured by photothermal deflection spectroscopy (PDS) between 1.5 and 3.5 eV, was reported by De Wolf et al.[6] Recently, also the complex refractive index in the visible was obtained from ellipsometry data, however, without providing experimental details.[12] Because ellipsometric data of thin films are inherently affected by multiple reflections and interferences, an accurate and reliable description of thin film optical properties requires
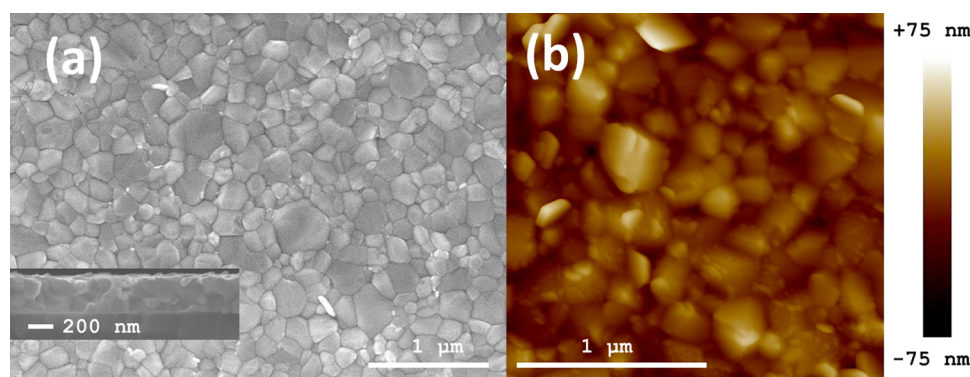
Figure 1. Scanning electron micrographs in top view (a) and cross section (inset) and atomic force micrograph (b) of the investigated film. Both images show a conformal morphology of the film with typical grain sizes of 100 to 300 nm.

modeling of the dielectric function (complex refractive index) to fit the ellipsometric and spectrophotometric data. (Let us remind that the complex refractive index, $N = n - ik$, contains the same information as the dielectric function, $\varepsilon = \varepsilon_1 - i\varepsilon_2$, with $\varepsilon_1 = n^2 - k^2$ and $\varepsilon_2 = 2nk$. While the dielectric function is closely related to the material's band structure, the refractive index is commonly used to describe the response of the material to light. Hereinafter, we use the terms synonymously depending on the context but refer to "dielectric function" when describing the theory and the model.) Optical analysis of complete $CH_3NH_3PbI_3$ solar cells and the $CH_3NH_3PbI_3$ layers therein was reported,[27,28] but the complex sample structures involved might have compromised the uniqueness of the fit and required a large number of free parameters.

We determine the complex refractive index (dielectric function) of $CH_3NH_3PbI_3$ at room temperature by simultaneous fitting to variable-angle spectroscopic ellipsometry (VASE) and spectrophotometry (UVVis) data. To the best of our knowledge, this is the first accurate and unambiguous determination of the complex refractive index of $CH_3NH_3PbI_3$.

In general, ellipsometry is based on determining the change in polarization state, that is, the complex reflection coefficients for perpendicular (s-) and parallel (p-) polarization, r_s and r_p, respectively, upon reflection at an interface between two media. Because r_s and r_p are material-specific parameters that depend directly on the dielectric function of the material, spectroscopic ellipsometry is a powerful tool to determine the dielectric function over a broad spectral range. Detailed information can be found in ref 29. The dielectric function is obtained indirectly by fitting a dielectric function model to the experimental data, taking into account all external parameters such as the incident angle, the sample structure, and surface roughness. To increase the accuracy and reliability of the results, reflectance and transmittance spectra can be included in the modeling and fitting procedure. Such a combined approach enhances the uniqueness of the fit[30] and allows for a direct comparison of the fitted model with the more intuitively accessible reflectance and transmittance spectra.

$CH_3NH_3PbI_3$ films consist of nanocrystals with reported grain sizes between 10 and 500 nm.[31−34] Surface roughness in the order of 5 to 100 nm is common,[32,34,35] and also large void volume fractions have been observed for some preparation routes.[32] Surface roughness and voids cause light depolarization and thus affect the information content of ellipsometric data, which might lead to ambiguous results. We attribute the fact that a thorough optical characterization of $CH_3NH_3PbI_3$ based

on ellipsometry has not been reported so far to the difficulties arising from the surface roughness and the nanomorphology. To determine the dielectric functions unequivocally, we used a simple sample structure and a $CH_3NH_3PbI_3$ layer that was optimized toward conformal and planar film deposition and characterized its surface morphology independently with scanning electron microscopy (SEM) and atomic force microscopy (see Methods).

Scanning electron micrographs in top view and cross section view (Figure 1a) as well as AFM scans (Figure 1b) confirmed that the film was conformal and spatially homogeneous. The vertical root-mean-square roughness derived from AFM scans is R_q = 14 nm.

We model the film as a double layer consisting of a bulk layer with thickness d_{Bulk} and a surface roughness layer with thickness d_{Rough}, as sketched in Figure 2. To model the surface roughness,
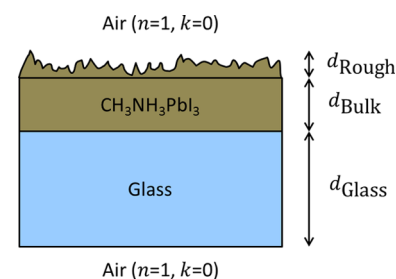

Figure 2. Sample structure used for the optical model.

we employ the approach introduced by Aspnes et al.,[36] which assumes an effective medium consisting of 50% air ($n = 1$, $k = 0$) and 50% film, using the Bruggeman effective medium approximation.[37]

To take the nanocrystalline nature of the $CH_3NH_3PbI_3$ films into account, we use the Forouhi–Bloomer[38] model in the parametrization of Jobin Yvon[39] ("new amorphous") for the complex refractive index (see Methods).

The ellipsometry spectra and the reflectance and transmittance, all acquired with light incidence from the film side, are plotted in Figure 3 (symbols).

The most prominent feature in the optical spectra is the well-known absorption edge at ∼1.55 eV, seen in Figure 3b as a sharp drop in transmittance at a wavelength of ∼800 nm. In the region of strong absorption, I_S approximately resembles the spectral features of the extinction coefficient, k. In this spectral region, that is, for $CH_3NH_3PbI_3$ at photon energies between 2 and 4 eV, two clear absorption peaks located at ∼2.5 and ∼3.5
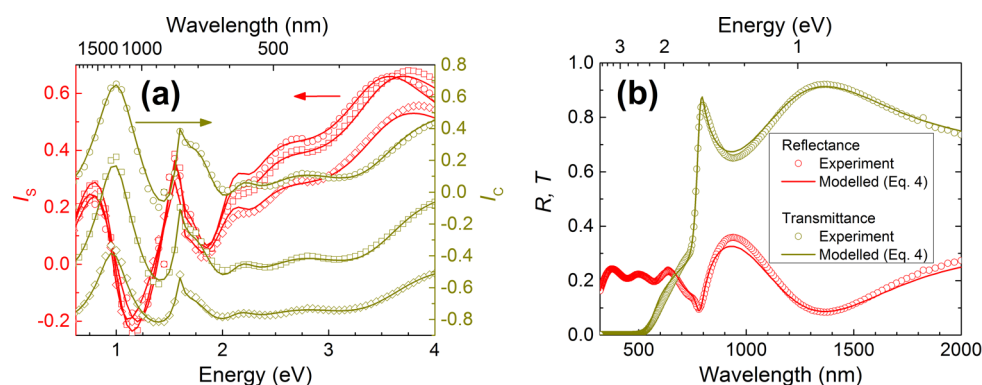
Figure 3. VASE spectra (a) for the measurement angles of 50 (diamonds), 60 (squares), and 70° (circles) and reflectance and transmittance spectra (b) along with the results of the dielectric function model of eq 4 (lines) fitted to the data (symbols). The dielectric function parameters are listed in Table 1.

eV are apparent in the ellipsometry spectra (Figure 3a). We remark that similar absorption peak positions were also reported by Hirasawa et al.[40] for the orthorhombic $CH_3NH_3PbI_3$ phase at 4.2 K, and transitions at 1.63 and 2.58 eV at room temperature were reported by Xing et al.[41]

On the basis of this empirical evidence, we fit the experimental spectra using the dielectric function of eq 4 (see Methods) with three oscillators having initial positions at 1.5, 2.5, and 3.5 eV.

The fit results are plotted in Figure 3 as lines together with the experimental data shown as symbols. All fit parameters are listed in Table 1. Over the full measured spectral range,

Table 1. Dielectric Function (eq 4) Parameters of the Best Fit to the Data (cf. Figure 3), Corresponding to $\chi^2 = 5.49$ (see Methods)

model parameter	fit result
d_{Rough}	10.56 nm
d_{Bulk}	300.4 nm
n_∞	1.990
E_g	1.553 eV
f_1	0.149
E_1	1.597 eV
Γ_1	0.080 eV
f_2	0.078
E_2	2.418 eV
Γ_2	0.387 eV
f_3	0.056
E_3	3.392 eV
Γ_3	0.448 eV

excellent agreement between the experimental data and the model can be observed ($\chi^2 = 5.49$, see Methods). To check our model for redundant parameters, we also tried to reproduce the experimental data with a lower number of oscillators. It is possible to obtain some agreement in restricted spectral ranges with only one or two oscillators, which stay close to the positions mentioned above. However, a reasonable fit over the full spectral range between 0.6 and 4 eV requires three oscillators. Figure 3 illustrates that our model reproduces all features of the experimental spectra; that is, there is no need to introduce more oscillators or other components to the dielectric function model.

The film thickness and surface roughness were treated as free parameters in the fitting procedure. The values of $d_{Bulk} = 300.4$

nm and $d_{Rough} = 10.6$ nm obtained from the fit are in excellent agreement with the independently measured values of 299.3 nm (obtained by profilometry) and 14 nm (obtained by AFM) for the thickness and roughness, respectively, further underlining the robustness of the result.

The refractive index spectra (n, k) of the bulk material, calculated from the final fit, is plotted in Figure 4a. The three oscillators are clearly visible as peaks in the extinction coefficient.

For temperatures of 4.2 K, Hirasawa et al. reported exciton energies of 1.633, 2.8, and 3.8 eV measured by diffuse reflectance.[40] Moreover, the 1.633 eV absorption peak is known to blueshift as the temperature increases to the orthorhombic-tetragonal phase transition at ~170 K[42,43] and then to redshift again upon further heating.[42,44] Additionally, the absorption loses its excitonic character as the temperature increases and k_BT is in the range of the exciton binding energy. Values in the range of 37[26] to 50 meV[42,45] were reported for the latter. Recently, very similar transitions energies, 1.63 and 2.58 eV, were reported by Xing et al. based on transient absorption measurements for $CH_3NH_3PbI_3$ at room temperature.[41] In view of these results, we conclude that the oscillator positions reported in Table 1 correspond to the same electronic transitions that were observed before by Hirasawa et al.[40] and Xing et al.[41]

Please note that the complex refractive index spectra published recently in refs 25 and 12 resemble our result only approximately (Figure 4), deviating considerably in both the magnitude of n and k and the spectral shape. The real part of the refractive index assumes a value of 2.61 at a wavelength of 633 nm, implying that $CH_3NH_3PbI_3$ is ideally suited as an antireflective coating for silicon solar cells. This is a remarkable result, as it underlines the promise of monolithic $CH_3NH_3PbI_3$/silicon tandem solar cells with potential efficiencies beyond the fundamental conversion limit of silicon photovoltaics.[20]

Figure 4b compares the absorption coefficient calculated according to $\alpha = 4\pi k/\lambda$, with λ being the wavelength, along with the absorption coefficient directly measured by PDS.[6] The two spectra are in very good agreement over the full spectral range of interest. In particular, the absorption edge measured by PDS is reproduced remarkably well by the model dielectric function reported here (Figure 4b inset), with excellent agreement down to values of $\alpha = 10^4$ cm^{-1} ($k = 0.01$). The model result also reproduces the kink at 2.5 eV that is apparent in the PDS measurement, however not as prominently. Please
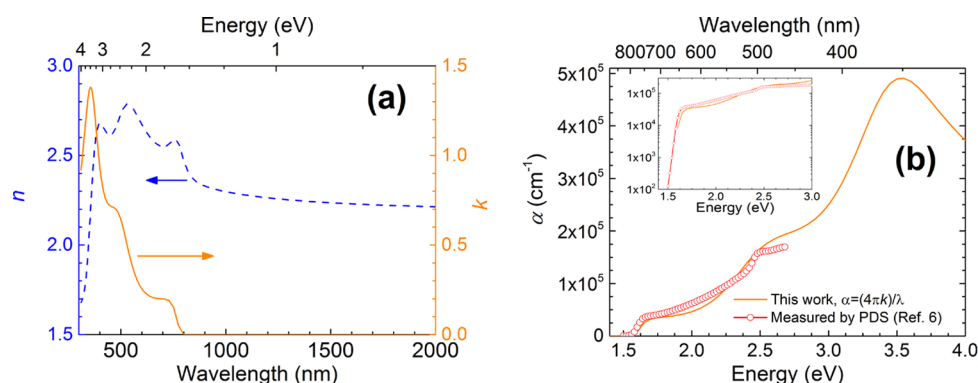
Figure 4. Refractive index (a) and absorption coefficient (b).

note that our result also reproduces all spectral features of the room temperature absorbance spectrum reported by Kitazawa et al.[46] between the energy of the bandgap and 4 eV, including the kink at 2.5 eV, the pronounced increase around 3 eV, the peak at 3.5 eV, and the decrease between 3.5 and 4 eV.

Figure 5 shows the dielectric function $(\varepsilon_1, \varepsilon_2)$ calculated with the parameters in Table 1.

Figure 5. Dielectric function $(\varepsilon_1, \varepsilon_2)$ of $CH_3NH_3PbI_3$ calculated with eq 4 (Methods) and the parameter set of Table 1 (corresponding to the fit shown in Figure 3).

For the real part of the dielectric constant, a value of $\varepsilon_1 = 6.5$ at a temperature of 4.2 K was derived,[26] which is in very good agreement with our result.

In conclusion, we have presented the first accurate determination of the complex refractive index (dielectric function) of $CH_3NH_3PbI_3$ based on simultaneously fitting variable-angle ellipsometry, reflectance, and transmittance spectra. Our model consists of three oscillators according to the Forouhi−Bloomer formulation that are centered at 1.597, 2.418, and 3.392 eV, and are consistent with Kramers−Kronig transformations. The result describes all features within the spectral range of 0.6 to 4 eV (λ = 300 to 2000 nm) and agrees well with previously reported data. The real part of the refractive index at 633 nm is 2.61, rendering $CH_3NH_3PbI_3$ ideally suited as an antireflection coating for silicon solar cells. This underlines the promise of $CH_3NH_3PbI_3$/Si tandem solar cells with potential efficiencies beyond the fundamental conversion limit of silicon photovoltaics. We believe that our results will help to further improve the design and modeling of perovskite-based optoelectronic devices.

■ METHODS

Sample Preparation. Thin $CH_3NH_3PbI_3$ films were prepared according to a procedure described by Jeon et al.[34] Lead iodide (PbI_2) and methylammonium iodide (CH_3NH_3I) with a concentration of 1.4 M and a molar ratio of 1:1 were dissolved at 60 °C in a 7:3 v/v γ-butyrolactone/dimethyl sulfoxide mixture. After the solution cooled to room temperature, it was spin-coated on a 500 μm thick cleaned Schott AF 32 glass substrate. Five seconds before the end of the last spin coating step, toluene was dripped onto the rotating sample, which resulted in an improved uniformity of the $CH_3NH_3PbI_3$ crystal growth. The sample was then annealed at 100 °C for 10 min. Solution processing and thermal annealing were performed in a N_2 atmosphere.

Sample Characterization. Ellipsometry measurements were carried out with a Horiba Jobin Yvon UVISEL iHR320 ellipsometer[47] under incident angles of 50, 60, and 70° for photon energies between 0.6 and 6 eV with 50 meV increment. Reflectance and transmittance spectra were measured with a PerkinElmer Lambda 950 spectrophotometer between 320 and 2000 nm with 10 nm increment. All measurements were done at room temperature (∼298 K). The film morphology and surface roughness were characterized with a Bruker Dimension Icon atomic force microscope, and the film thickness was determined with a KLA Tencor P16+ profilometer. The film morphology was determined with a JEOL JSM-7500TFE SEM.

The directly measured quantities in polarization modulation ellipsometers are the first and second harmonics of the base modulation frequency of the polarized light, I_s and I_C, after reflection from the sample surface[29]

$$I = I_1(I_0 + I_s \sin(\delta) + I_C \cos(\delta)) \qquad (1)$$

I is the total light intensity, I_1 and I_0 are time-independent parameters, and δ is the time-dependent phase. Ellipsometric data are frequently expressed by the amplitude ratio ψ and phase difference Δ between s- and p-polarization

$$\tan(\psi) = |r_p|/|r_s| \quad \Delta = \delta_{rp} - \delta_{rs'} \qquad (2)$$

where $|r_p|$ and $|r_s|$ are the amplitude of the reflection coefficient for p- and s-polarization, respectively, and δ_{rp} and δ_{rp} are their respective phases. These quantities are parametrizations of I_s and I_C

$$I_s = 2\mathrm{Im}\left(\frac{r_s r_p^*}{r_s r_s^* + r_p r_p^*}\right) = \sin(2\psi)\sin(\Delta)$$

$$I_C = 2\mathrm{Re}\left(\frac{r_s r_p^*}{r_s r_s^* + r_p r_p^*}\right) = \sin(2\psi)\sin(\Delta) \tag{3}$$

To take the nanocrystalline nature of the $CH_3NH_3PbI_3$ films into account, we use the Forouhi−Bloomer[38] model in the parametrization of Jobin Yvon[39] ("new amorphous") for the complex refractive index,

$$n(E) = n_\infty + \sum_{j=1}^{N} \frac{B_j(E - E_j) + C_j}{(E - E_j)^2 + \Gamma_j^2};$$

$$k(E) = \begin{cases} \sum_{j=1}^{N} \dfrac{f_j(E - E_g)^2}{(E - E_j)^2 + \Gamma_j^2}; & \text{for } E > E_g \\ 0; & \text{for } E > E_g \end{cases} \tag{4}$$

with

$$B_j = \frac{f_j}{\Gamma_j}(\Gamma_j^2 - (E_j - E_g)^2)$$

$$C_j = 2f_j \Gamma_j (E_j - E_g)$$

E is the energy, E_g is the bandgap, and E_j, f_j, and Γ_j are the position, strength, and width of one oscillator. Please note that the Forouhi−Bloomer model is Kramers−Kronig consistent.

■ ASSOCIATED CONTENT

Ⓢ Supporting Information

The complex refractive index, the dielectric function, and the absorption coefficient are available in tabular form. This material is available free of charge via the Internet at http://pubs.acs.org.

■ AUTHOR INFORMATION

Corresponding Author
*E-mail: philipp.loeper@epfl.ch. Tel: +41-21-6954562.

Notes
The authors declare no competing financial interest.

■ ACKNOWLEDGMENTS

■ REFERENCES

(1) NREL Efficiency Chart. http://www.nrel.gov/ncpv/images/efficiency_chart.jpg (accessed 17.11.2014).

(2) Kojima, A.; Teshima, K.; Miyasaka, T.; Shirai, Y. *Novel Photoelectrochemical Cell with Mesoscopic Electrodes Sensitized by Lead-Halide Compounds (2)*; 210th ECS Meeting; The Electrochemical Society: Pennington, NJ, 2006; p 397

(3) Green, M. A.; Ho-Baillie, A.; Snaith, H. J. The Emergence of Perovskite Solar Cells. *Nat. Photonics* **2014**, *8*, 506−514.

(4) Kim, H.-S.; Lee, C.-R.; Im, J.-H.; Lee, K.-B.; Moehl, T.; Marchioro, A.; Moon, S.-J.; Humphry-Baker, R.; Yum, J.-H.; Moser, J. E.; Grätzel, M.; Park, N.-G. Lead Iodide Perovskite Sensitized All-Solid-State Submicron Thin Film Mesoscopic Solar Cell with Efficiency Exceeding 9%. *Sci. Rep.* **2012**, *2*, 1−7.

(5) Eperon, G. E.; Stranks, S. D.; Menelaou, C.; Johnston, M. B.; Herz, L. M.; Snaith, H. J. Formamidinium Lead Trihalide: A Broadly Tunable Perovskite for Efficient Planar Heterojunction Solar Cells. *Energy Environ. Sci.* **2014**, *7*, 982−988.

(6) De Wolf, S.; Holovsky, J.; Moon, S.-J.; Löper, P.; Niesen, B.; Ledinsky, M.; Haug, F.-J.; Yum, J.-H.; Ballif, C. Organometallic Halide Perovskites: Sharp Optical Absorption Edge and Its Relation to Photovoltaic Performance. *J. Phys. Chem. Lett.* **2014**, *5*, 1035−1039.

(7) Snaith, H. J. Perovskites: The Emergence of a New Era for Low-Cost, High-Efficiency Solar Cells. *J. Phys. Chem. Lett.* **2013**, *4*, 3623−3630.

(8) Topic, M.; Geisthardt, R. M.; Sites, J. R. Performance Limits and Status of Single-Junction Solar Cells with Emphasis on Cigs. *IEEE J. Photovol.* **2014**, 1−6.

(9) Tan, Z.-K.; Moghaddam, R. S.; Lai, M. L.; Docampo, P.; Higler, R.; Deschler, F.; Price, M.; Sadhanala, A.; Pazos, L. M.; Credgington, D.; Hanusch, F.; Bein, T.; Snaith, H. J.; Friend, R. H. Bright Light-Emitting Diodes Based on Organometal Halide Perovskite. *Nat. Nanotechnol.* **2014**, *9*, 687−692.

(10) Deschler, F.; Price, M.; Pathak, S.; Klintberg, L. E.; Jarausch, D.-D.; Higler, R.; Hüttner, S.; Leijtens, T.; Stranks, S. D.; Snaith, H. J.; Atatüre, M.; Phillips, R. T.; Friend, R. H. High Photoluminescence Efficiency and Optically Pumped Lasing in Solution-Processed Mixed Halide Perovskite Semiconductors. *J. Phys. Chem. Lett.* **2014**, *5*, 1421−1426.

(11) Dhanker, R.; Brigeman, A. N.; Larsen, A. V.; Stewart, R. J.; Asbury, J. B.; Giebink, N. C. Random Lasing in Organo-Lead Halide Perovskite Microcrystal Networks. *Appl. Phys. Lett.* **2014**, *105*, 151112.

(12) Xing, G.; Mathews, N.; Lim, S. S.; Yantara, N.; Liu, X.; Sabba, D.; Grätzel, M.; Mhaisalkar, S.; Sum, T. C. Low-Temperature Solution-Processed Wavelength-Tunable Perovskites for Lasing. *Nat. Mater.* **2014**, *13*, 476−480.

(13) Sutherland, B. R.; Hoogland, S.; Adachi, M. M.; Wong, C. T. O.; Sargent, E. H. Conformal Organohalide Perovskites Enable Lasing on Spherical Resonators. *ACS Nano* **2014**, *8*, 10947−10952.

(14) Kagan, C. R.; Mitzi, D. B.; Dimitrakopoulos, C. D. Organic-Inorganic Hybrid Materials as Semiconducting Channels in Thin-Film Field-Effect Transistors. *Science* **1999**, *286*, 945−947.

(15) Mitzi, D. B.; Chondroudis, K.; Kagan, C. R. Organic-Inorganic Electronics. *IBM J. Res. Dev.* **2001**, *45*, 29−45.

(16) Cheng, Z.; Lin, J. Layered Organic−Inorganic Hybrid Perovskites: Structure, Optical Properties, Film Preparation, Patterning and Templating Engineering. *CrystEngComm* **2010**, *12*, 2646.

(17) Todorov, T.; Gershon, T.; Gunawan, O.; Sturdevant, C.; Guha, S. Perovskite-Kesterite Monolithic Tandem Solar Cells with High Open-Circuit Voltage. *Appl. Phys. Lett.* **2014**, *105*, 173902.

(18) Löper, P.; Moon, S.-J.; Nicolas, S. M. d.; Niesen, B.; Ledinsky, M.; Nicolay, S.; Bailat, J.; Yum, J.-H.; Wolf, S. D.; Ballif, C. Organic-Inorganic Halide Perovskite/Crystalline Silicon Four-Terminal Tandem Solar Cells. *Phys. Chem. Chem. Phys.* **2014**, DOI: 10.1039/C4CP03788J.

(19) Löper, P.; Niesen, B.; Moon, S.; Martin de Nicolas, S.; Holovsky, J.; Remes, Z.; Ledinsky, M.; Haug, F.; Yum, J.; De Wolf, S.; Ballif, C. Organic-Inorganic Halide Perovskites: Perspectives for Silicon-Based Tandem Solar Cells. *IEEE J. Photovoltaics* **2014**, *4*, 1545−1551.

(20) Schneider, B. W.; Lal, N. N.; Baker-Finch, S.; White, T. P. Pyramidal Surface Textures for Light Trapping and Antireflection in Perovskite-on-Silicon Tandem Solar Cells. *Opt. Express* **2014**, *22*, A1422−A1430.

(21) Lal, N. N.; White, T. P.; Catchpole, K. R. Optics and Light Trapping for Tandem Solar Cells on Silicon. *IEEE J. Photovoltaics* **2014**, *4*, 1380−1386.

(22) Onoda-Yamamuro, N.; Matsuo, T.; Suga, H. Dielectric Study of CH3NH3PbX3 (X=Cl, Br, I). *J. Phys. Chem. Solids* **1992**, *53*, 935−939.

(23) Maeda, M.; Hattori, M.; Hotta, A.; Suzuki, I. Dielectric Studies on CH3NH3Pbx3 (X=Cl and Br) Single Cystals. *J. Phys. Soc. Jpn.* **1997**, *66*, 1508−1511.

(24) Juarez-Perez, E. J.; Sanchez, R. S.; Badia, L.; Garcia-Belmonte, G.; Kang, Y. S.; Mora-Sero, I.; Bisquert, J. Photoinduced Giant Dielectric Constant in Lead Halide Perovskite Solar Cells. *J. Phys. Chem. Lett.* **2014**, *5*, 2390−2394.

(25) Poglitsch, A.; Weber, D. Dynamic Disorder in Methylammoniumtrihalogenoplumbates (Ii) Observed by Millimeter-Wave Spectroscopy. *J. Chem. Phys.* **1987**, *87*, 6373−6378.

(26) Hirasawa, M.; Ishihara, T.; Goto, T.; Uchida, K.; Miura, N. Magnetoabsorption of the Lowest Exciton in Perovskite-Type Compound (CH3NH3)PbI3. *Phys. B* **1994**, *201*, 427−430.

(27) Chen, C.-W.; Hsiao, S.-Y.; Chen, C.-Y.; Kang, H.-W.; Huang, Z.-Y.; Lin, H.-W. Optical Properties of Organometal Halide Perovskite Thin Films and General Device Structure Design Rules for Perovskite Single and Tandem Solar Cells. *J. Mater. Chem. A* **2014**, DOI: 10.1039/C4TA05237D.

(28) Anaya, M.; Lozano, G.; Calvo, M. E.; Zhang, W.; Johnston, M. B.; Snaith, H. J.; Míguez, H. Optical Description of Mesostructured Organic-Inorganic Halide Perovskite Solar Cells. *J. Phys. Chem. Lett.* **2015**, 48−53.

(29) Fujiwara, H. *Spectroscopic Ellipsometry: Principles and Applications*; John Wiley & Sons: Chichester, U.K., 2007; p 390.

(30) Hilfiker, J. N.; Synowicki, R. A.; Tompkins, H. G. *Spectroscopic Ellipsometry Methods for Thin Absorbing Coatings*, Proceedings of the 51st Annual Technical Conference - Society of Vacuum Coaters, Chicago; Society of Vacuum Coaters: Chicago, 2008; pp 511−516.

(31) Liu, M.; Johnston, M. B.; Snaith, H. J. Efficient Planar Heterojunction Perovskite Solar Cells by Vapour Deposition. *Nature* **2013**, *501*, 395−8.

(32) Burschka, J.; Pellet, N.; Moon, S.-J.; Humphry-Baker, R.; Gao, P.; Nazeeruddin, M. K.; Grätzel, M. Sequential Deposition as a Route to High-Performance Perovskite-Sensitized Solar Cells. *Nature* **2013**, *499*, 316−319.

(33) Chen, Q.; Zhou, H.; Hong, Z.; Luo, S.; Duan, H. S.; Wang, H. H.; Liu, Y.; Li, G.; Yang, Y. Planar Heterojunction Perovskite Solar Cells Via Vapor-Assisted Solution Process. *J. Am. Chem. Soc.* **2014**, *136*, 622−5.

(34) Jeon, N. J.; Noh, J. H.; Kim, Y. C.; Yang, W. S.; Ryu, S.; Seok, S. I. Solvent Engineering for High-Performance Inorganic−Organic Hybrid Perovskite Solar Cells. *Nat. Mater.* **2014**, *13*, 897−903.

(35) Malinkiewicz, O.; Yella, A.; Lee, Y. H.; Espallargas, G. M.; Graetzel, M.; Nazeeruddin, M. K.; Bolink, H. J. Perovskite Solar Cells Employing Organic Charge-Transport Layers. *Nat. Photonics* **2014**, *8*, 128−132.

(36) Aspnes, D. E.; Theeten, J. B.; Hottier, F. Investigation of Effective-Medium Models of Microscopic Surface Roughness by Spectroscopic Ellipsometry. *Phys. Rev. B* **1979**, *20*, 3292−302.

(37) Bruggeman, D. A. G. Berechnung Verschiedener Physikalischer Konstanten Von Heterogenen Substanzen. I. Dielektrizitätskonstanten Und Leitfähigkeiten Der Mischkörper Aus Isotropen Substanzen. *Ann. Phys.* **1935**, *416*, 636−64.

(38) Forouhi, A.; Bloomer, I. Optical Dispersion Relations for Amorphous Semiconductors and Amorphous Dielectrics. *Phys. Rev. B* **1986**, *34*, 7018−7026.

(39) JobinYvon New Amorphous Dispersion Formula. http://www.horiba.com/fileadmin/uploads/Scientific/Downloads/OpticalSchool_CN/TN/ellipsometer/New_Amorphous_Dispersion_Formula.pdf (accessed 14.11.2014).

(40) Hirasawa, M.; Ishihara, T.; Goto, T. Exciton Features in 0-, 2-, and 3-Dimensional Networks of [PbI6]4- Octahedra. *J. Phys. Soc. Jpn.* **1994**, *63*, 3870−3879.

(41) Xing, G.; Mathews, N.; Sun, S.; Lim, S. S.; Lam, Y. M.; Grätzel, M.; Mhaisalkar, S.; Sum, T. C. Long-Range Balanced Electron- and Hole-Transport Lengths in Organic-Inorganic CH3NH3PbI3. *Science* **2013**, *342*, 344−347.

(42) D'Innocenzo, V.; Grancini, G.; Alcocer, M. J.; Kandada, A. R.; Stranks, S. D.; Lee, M. M.; Lanzani, G.; Snaith, H. J.; Petrozza, A. Excitons Versus Free Charges in Organo-Lead Tri-Halide Perovskites. *Nat. Commun.* **2014**, *5*, 3586.

(43) Onoda-Yamamuro, N.; Matsuo, T.; Suga, H. Calorimetric and Ir Spectroscopic Studies of Phase Transitions in Methylammonium Trihalogenoplumbates (II)†. *J. Phys. Chem. Solids* **1990**, *51*, 1383−1395.

(44) Ishihara, T. Optical Properties of PbI-Based Perovskite Structures. *J. Lumin.* **1994**, *60−61*, 269−274.

(45) Tanaka, K.; Takahashi, T.; Ban, T.; Kondo, T.; Uchida, K.; Miura, N. Comparative Study on the Excitons in Lead-Halide-Based Perovskite-Type Crystals CH3NH3PbBr3 CH3NH3PbI3. *Solid State Commun.* **2003**, *127*, 619−623.

(46) Kitazawa, N.; Watanabe, Y.; Nakamura, Y. Optical Properties of CH3NH3PbX3 (X = Halogen) and Their Mixed-Halide Crystals. *J. Mater. Sci.* **2002**, *37*, 3585−3587.

(47) Stückelberger, M. *Hydrogenated Amorphous Silicon: Impact of Process Conditions on Material Properties and Solar Cell Efficiency*; École Polytechnique Fédérale de Lausanne (EPFL): Lausanne, Switzerland, 2014.